Insights into the electronic structure of OsO_2 using soft and hard x-ray photoelectron spectroscopy in combination with density functional theory

Anna Regoutz,[1,*] Alex M. Ganose,[2,3,4] Lars Blumenthal,[1,5] Christoph Schlueter,[3,†] Tien-Lin Lee,[3] Gregor Kieslich,[6] Anthony K. Cheetham,[7] Gwilherm Kerherve,[1] Ying-Sheng Huang,[8,‡] Ruei-San Chen,[9] Giovanni Vinai,[10] Tommaso Pincelli,[10] Giancarlo Panaccione,[10] Kelvin H. L. Zhang,[11] Russell G. Egdell,[12] Johannes Lischner,[1,5] David O. Scanlon,[2,3,4] and David J. Payne[1,§]

[1]*Department of Materials, Imperial College London, South Kensington, London SW7 2AZ, United Kingdom*
[2]*Department of Chemistry, University College London, 20 Gordon Street, London WC1H 0AJ, United Kingdom*
[3]*Diamond Light Source Ltd., Diamond House, Harwell Science and Innovation Campus, Didcot OX11 0DE, United Kingdom*
[4]*Thomas Young Centre, University College London, Gower Street, London WC1E 6BT, United Kingdom*
[5]*Thomas Young Centre for Theory and Simulation of Materials, United Kingdom*
[6]*Department of Chemistry, Technical University of Munich, Lichtenbergstraße 4, Garching, Germany*
[7]*Functional Inorganic and Hybrid Materials Group, Department of Materials Science & Metallurgy, University of Cambridge, 27 Charles Babbage Road, Cambridge CB3 0FS, United Kingdom*
[8]*Department of Electric Engineering, National Taiwan University of Science and Technology, Taipei 6, Taiwan*
[9]*Graduate Institute of Applied Science and Technology, National Taiwan University of Science and Technology, Taipei 106, Taiwan*
[10]*Laboratorio TASC, IOM-CNR, S.S. 14 km 163.5, Basovizza, I-34149 Trieste, Italy*
[11]*Department of Materials Science & Metallurgy, University of Cambridge, 27 Charles Babbage Road, Cambridge CB3 0FS, United Kingdom*
[12]*Inorganic Chemistry Laboratory, Department of Chemistry, University of Oxford, South Parks Road, Oxford OX1 3QR, United Kingdom*

(Received 4 October 2018; published 4 February 2019)

Theory and experiment are combined to gain an understanding of the electronic properties of OsO_2, a poorly studied metallic oxide that crystallizes in the rutile structure. Hard and soft valence-band x-ray photoemission spectra of OsO_2 single crystals are in broad agreement with the results of density-functional-theory calculations, aside from a feature shifted to high binding energy of the conduction band. The energy shift corresponds to the conduction electron plasmon energy measured by reflection electron energy loss spectroscopy. The plasmon satellite is reproduced by many-body perturbation theory.

DOI: 10.1103/PhysRevMaterials.3.025001

The physics of the heavier 5*d* transition metals has seen a surge of interest in the past decade, due to the coincidence of energy scales of spin-orbit coupling (SOC), crystal field splitting, and electron correlation effects. Research to date has focused heavily on iridates where magnetic instabilities, transitions from metallic to insulating states, the promise of topological insulating phases, superconductivity, and other exotic condensed matter physics continues to generate significant research activity [1,2]. In contrast, the physics of osmates is only now starting to be explored, principally where osmium exists in the +5 oxidation state (d^3). For example, the pyrochlore $Cd_2Os_2O_7$ has been shown to display a multiple-spin-flip magnetic excitation [3], and the perovskite $NaOsO_3$ has been shown to go through a metal-insulator transition, driven by magnetic correlations [4]. In addition, the double perovskites Ca_3LiOsO_6 and Ba_2YOsO_6 have been shown to host a spin-orbit entangled $J = 3/2$ electronic ground state [5,6]. Further systems continue to be reported, but as can be seen, in comparison to iridates, exploration of the condensed matter physics of osmates remains in its infancy.

In contrast to the ternary and quaternary osmates the binary oxide OsO_2 belongs to a group of transition-metal dioxides, including IrO_2, RuO_2, PtO_2, TcO_2, and ReO_2, which crystallize in the rutile structure and show metallic behavior [7–10]. Compared to the majority of SOC-driven 5*d* transition-metal oxides, the electronic structure of the rutile binaries can be explained with crystal-field arguments put forward by Goodenough [11]. Despite the conceptually simple explanation for the bulk electronic structure, there exists significant complexity and subtlety in the band structure which is waiting to be explored. For example, the electronic structure of IrO_2 and OsO_2 has been predicted to host Dirac nodal lines [12,13], a feature that has been theoretically proposed to be important for the spin Hall effect.

OsO_2 itself is a metallic low-spin d^4 compound with a reported room-temperature resistivity on the order of 1.5–6.0×10^{-5} Ω cm [14,15]. Very little is known about this oxide due to the difficulty of obtaining high-quality samples and its tendency to form OsO_4, a highly volatile and toxic compound, as on heating or sputtering OsO_2 readily disproportionates [16,17]. Therefore, experiments with OsO_2, and particularly surface science measurements, suffer from significant limitations regarding sample treatment and

*Corresponding author: a.regoutz@imperial.ac.uk
†Current address: Photon Science, Deutsches Elektronen Synchrotron DESY, Hamburg, Germany.
‡Deceased.
§Corresponding author: d.payne@imperial.ac.uk

 ©2019 American Physical Society

surface preparation, which has restricted the study of OsO_2 to date.

This work presents an in-depth study of OsO_2 single crystals by high-resolution soft and hard x-ray photoelectron spectroscopy (SXPS and HAXPES), in combination with reflection electron energy loss spectroscopy (REELS). Experiments are complemented by theoretical calculations within the framework of density functional theory (DFT) and many-body perturbation theory within the "GW plus cumulant" (GW+C) approach. Based on this holistic approach, a detailed overview and some insights into the electronic structure of OsO_2 are provided.

Single crystals of OsO_2 were prepared by oscillating chemical vapor transport as described in detail elsewhere [15]. Crystals of several mm in size were obtained which are coppery-brown with a gold luster. The structural purity of the samples was confirmed by using powder x-ray diffraction (PXRD). Powder x-ray diffraction data of finely ground powder of OsO_2 were collected on a Bruker D8, using CuKα radiation and a 2θ step size of 0.01943°. Profile fitting and subsequent Rietveld refinement have been performed using TOPAS Academic, v5.0. The x-ray photoelectron spectra were recorded at two facilities. Laboratory-based XPS on the single crystals was conducted at Imperial College (London, UK) on a Thermo Scientific K-Alpha$^+$ x-ray photoelectron spectrometer (base pressure 2×10^{-9} mbar), incorporating a monochromated, microfocused Al Kα x-ray source (hν = 1486.6 eV) and a 180° double focusing hemispherical analyzer with two-dimensional detector. The x-ray source was operated at 6 mA emission current and 12-kV anode bias. Data were collected using a 400 μm x-ray spot and a pass energy of 200 eV for survey and 20 eV for core level and valence-band spectra. HAXPES were collected at the I09 beamline at the Diamond Light Source, UK. A double-crystal Si (111) monochromator was used to select 2.50-, 5.93-, and 8.14-keV photons, which for simplicity will be further referred to as 2.5, 6, and 8 keV. The resulting total experimental resolution was evaluated at each energy by measuring the Fermi edge of a polycrystalline gold reference sample and fitting the data to a Gaussian-broadened Fermi-Dirac distribution. To ensure a comparable energy resolution of 250–300 meV for all energies, Si (004) and Si (044) channel-cut crystals were employed as a postmonochromator for the measurements at 5.93 and 8.14 keV. The end station is equipped with a VG Scienta EW4000 electron analyzer with ±30° angular acceptance. REELS data were recorded on a Thermo Scientific NEXSA XPS system using its flood gun as a primary electron gun with a beam energy of 980 eV and an emission current of 5 μA. The system uses a 180° double focusing hemispherical analyzer with a two-dimensional detector to measure the backscattered electrons at a pass energy of 5 eV.

Density-functional theory, as implemented in the Vienna Ab initio Simulation Package (VASP), was employed for the calculations of the band structure and density of states [18–21]. VASP is a plane-wave DFT code in which the interactions between the core and valence electrons are described using the projector augmented wave method [22]. This study employed the PBEsol functional [23] a version of the Perdew-Burke-Ernzerhof (PBE) [24] functional reparameterized for solids, which has been shown to accurately predict the lattice parameters for similar rutile systems [25,26]. For the six-atom unit cell of OsO_2, a plane-wave energy cut-off of 450 eV and $12 \times 12 \times 16$ k-point mesh centered at the Γ point of the first Brillouin zone were required to achieve convergence. The unit cell was geometrically relaxed until the forces on all atoms totalled less than 10 meV Å^{-1}. When calculating electronic properties, special attention was paid to relativistic effects through use of scalar relativistic pseudopotentials and explicit treatment of SOC [27].

To capture many-electron effects beyond DFT, many-body perturbation theory calculations using the GW+C approach were carried out. In recent years, the GW+C approach has been established as the state-of-the-art method to simulate photoemission spectra of bulk solids and nanomaterials with weak or moderate electron correlations [28–36]. Notably, this approach accurately describes both quasiparticle and plasmon satellite features in the electron spectral function, which is measured in photoemission experiments. However, few applications of the GW+C approach to oxide materials have been reported in the literature [33,34,37].

In the GW+C approach, the spectral function of an electron in band n with crystal momentum $\mathbf{k}$ is given by [29]

$$A_{n\mathbf{k}}(\omega) = \frac{e^{-a_{n\mathbf{k}}}}{\pi} \sum_{m=0}^{\infty} \frac{a_{n\mathbf{k}}^m}{m!} \frac{\gamma_{n\mathbf{k}}}{(\omega - E_{n\mathbf{k}} + m\omega_{\mathrm{pl}})^2 + \gamma_{n\mathbf{k}}^2}, \quad (1)$$

where $E_{n\mathbf{k}}$ and $\gamma_{n\mathbf{k}}$ denote the quasiparticle energy and linewidth, respectively; ω_{pl} is the plasmon energy at small wave vectors; and $a_{n\mathbf{k}} = (1 - Z_{n\mathbf{k}})/Z_{n\mathbf{k}}$ with $Z_{n\mathbf{k}}$ being the quasiparticle renormalization factor.

To evaluate Eq. (1), we obtained $E_{n\mathbf{k}}$ and $Z_{n\mathbf{k}}$ using G_0W_0 calculations as implemented in the BerkeleyGW programme package [38]. As mean-field starting point, we used a DFT-PBE calculation [39] and then computed the electron self-energy using a 40-Ry cutoff for the screened Coulomb interaction and a summation over 1500 Kohn-Sham states. Finally, the experimentally measured plasmon energy is used in Eq. (1). We have also calculated the plasmon energy using the random-phase approximation and found that this overestimates ω_{pl} by a few tenths of an eV.

Figure 1 shows the PXRD measurement including the result of the Rietveld refinement. In good agreement with previous reports, OsO_2 crystallizes in the well-known rutile structure (see inset in Fig. 1), with lattice parameters of a = 4.49907(3)Å and c = 3.18555(5)Å [14,16,40]. The structure parameters found for the present samples, literature values, and the values derived from theory are summarized in Table I. The x value of the observed oxygen position is 0.3044(2), which is in good agreement with the calculated value of 0.30884.

Photoelectron spectroscopy of the core levels of OsO_2 provide an opportunity to interrogate the electronic structure of the material. The overlapping Os 4f and 5p core levels of OsO_2 [see Fig. 2(a)] show a strong response to a change in excitation energy, as would be expected from their theoretical cross sections (see Fig. 1 in the Supplemental Material for Os and O cross sections calculated using the Galore software package) [41,42]. The Os 4f cross section decays more rapidly on an increase in photon energy compared to the 5p one, leading to a crossover at around 2.6 keV. This

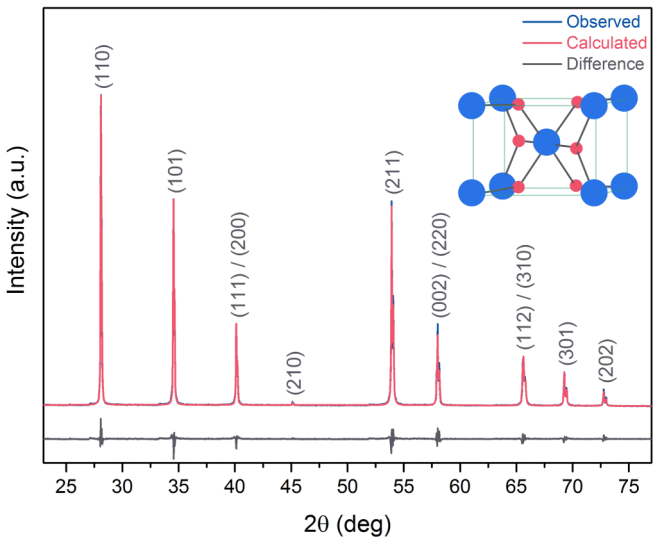

FIG. 1. Powder x-ray diffraction pattern and Rietveld refinement of OsO_2. The inset shows the unit cell of rutile, with the blue spheres representing Os and the red spheres representing O.

results in a dramatic increase with the photon energy of the contribution from Os $5p$ close to the $4f$ core level. The core levels show a distinctly asymmetric line shape due to the metallic nature of OsO_2, which has been observed in two previous reports on these core lines [15,43]. Asymmetry in the core levels of metallic metal oxides can be attributed to conduction electron screening effects [44–50]. The best peak fits [see Fig. 2(b) for a representative peak fit] were obtained by describing each line using two separate contributions: a main line combined with a higher binding energy feature referred to as the satellite (sat) line. Overall, while the $4f$ line is indeed very sharp with a full width half maximum (FWHM) of less than 0.5 eV, the $5p$ lines are much broader with a FWHM of larger than 1.5 eV. The spin orbit splitting

TABLE I. Crystal structure parameters from the literature [14,16,40] from Rietveld refinement of PXRD data and from DFT calculations. a and c are the lattice parameters, $\frac{c}{a}$ is their ratio, and V is the unit cell volume.

	Ref. [14]	Ref. [16]	Ref. [40]	PXRD	DFT
a/Å	4.4968	4.5003	4.5004	4.49907(3)	4.4723
c/Å	3.1820	3.1839	3.1819	3.18555(5)	3.1907
$\frac{c}{a}$	0.7076	0.7075	0.7070	0.70804(6)	0.7134
V/Å^3	64.34	64.48	64.44	64.48	63.82

for the $4f$ pair could be exactly determined to be 2.7 eV, with binding energies of 51.2 and 53.9 eV for $4f_{7/2}$ and $4f_{5/2}$, respectively. The separations between the main peaks and the satellites were found to be close to the conduction electron plasmon energy, to be discussed in more detail below (the satellite separations were 2.1 eV for $4f_{7/2}$ and 1.9 eV for $4f_{5/2}$, as compared to a plasmon energy of 1.85 eV). Due to the very low cross section for the $5p$ line in commonly used soft XPS, no reliable experimental data are available for its spin orbit splitting. The use of HAXPES at high photon energies in the present case allows the extraction of a value of 12.0 ± 0.25 eV, with the uncertainty connected to the strong overlap between the main $5p_{1/2}$ component and the $4f_{5/2}$ satellite. This overlap made it impossible to perform a meaningful and robust decomposition of the $5p_{1/2}$ peak into its two expected components.

The electronic band structure and density of states of OsO_2, calculated using PBEsol+SOC, are shown in Fig. 3. The band structure confirms the metallic nature of OsO_2, with four bands crossing the Fermi level, in agreement with previous calculations [7]. The limited dispersion of these bands gives rise to a relatively large density of states at the Fermi level. It is also in good agreement with the recently reported band structure by Sun *et al.* [12], where they have predicted the presence of Dirac nodal lines in the band structures of a series

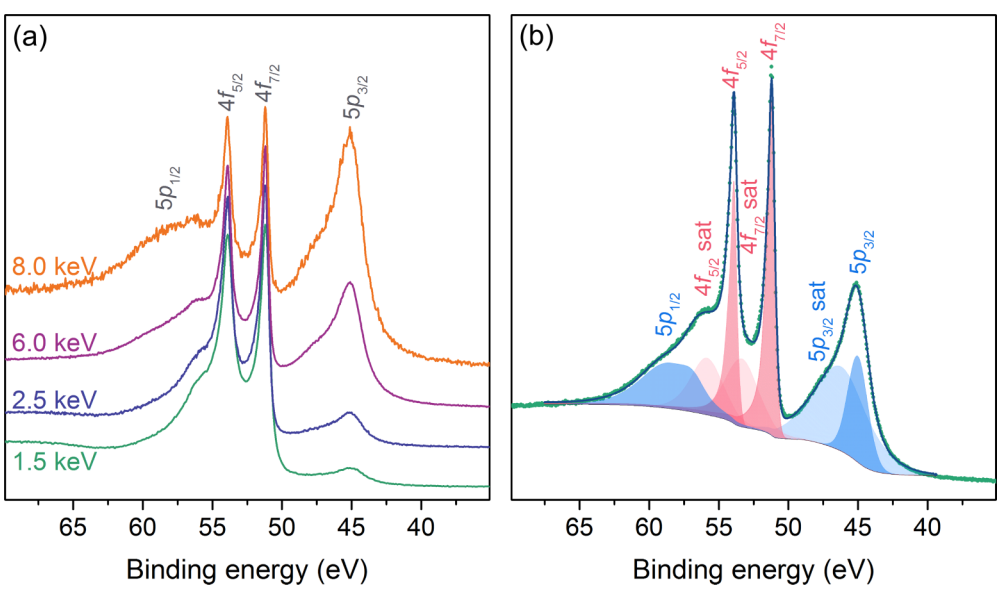

FIG. 2. The x-ray photoelectron spectra of the Os $4f$ and $5p$ core levels (a) collected at varying excitation energies and (b) peak fit of the spectrum at 6 keV.

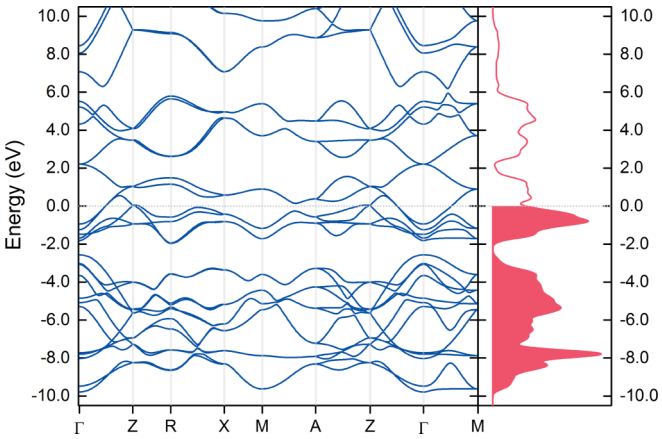

FIG. 3. Energy band structure and total density of states of OsO_2 calculated within density- functional theory (PBEsol) including spin-orbit coupling.

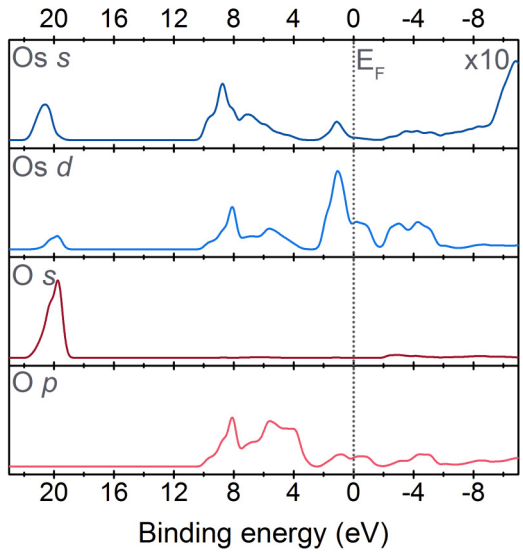

FIG. 5. PDOS for Os and O. The dotted line represents the Fermi energy E_F.

of metallic rutile oxides, including OsO_2, which are proposed to contribute to large spin Hall conductivity [51].

Only one experimental measurement of the valence band (VB) of OsO_2, obtained using Al Kα x-rays, has been reported in the literature [17], but the low energy resolution and poor signal-to-noise ratio prohibited a detailed investigation of the VB features. Therefore, Fig. 4(a) shows *high-resolution* valence band spectra measured across a range of photon energies hν, specifically 1.5, 2.5, 6, and 8 keV. The four spectra are normalized to their maxima to aid comparison. The valence band spectra look near identical across the different photon energies, as they are dominated by Os 5*d* states at all four energies due to the large 5*d* cross sections (see Fig. 1 in the Supplemental Material) [42]. Three major features are observed at 0.7 eV (I), 5.8 eV (II), and 8.2 eV (III). In Fig. 4(b), the valence band spectrum collected at h$\nu = 6$ keV is compared to the cross-section-weighted density of states from DFT calculations. We find good agreement between theory and experiment for the three major features I, II, and III. Analysis of the partial density of states (PDOS), shown in Fig. 5, reveals that feature I is dominated by Os 5*d* states with a small contribution from O 2*p* states. Features II and III consist of O 2*p* states hybridized with Os 5*d* states and a small contribution from Os 6*s* and 6*p* states.

In addition to these three major peaks, a small feature (marked with an asterisk in Fig. 4) at a binding energy of 2.7 eV is observed. The position of this additional feature is independent of photon energy and its binding energy position is 1.9 eV higher than that of feature I. Interestingly, this feature is not captured by the DFT DOS, suggesting that it originates from many-body effects, such as the excitation of a plasmon in response to the creation of a hole in the conduction band. To confirm this hypothesis, we have measured

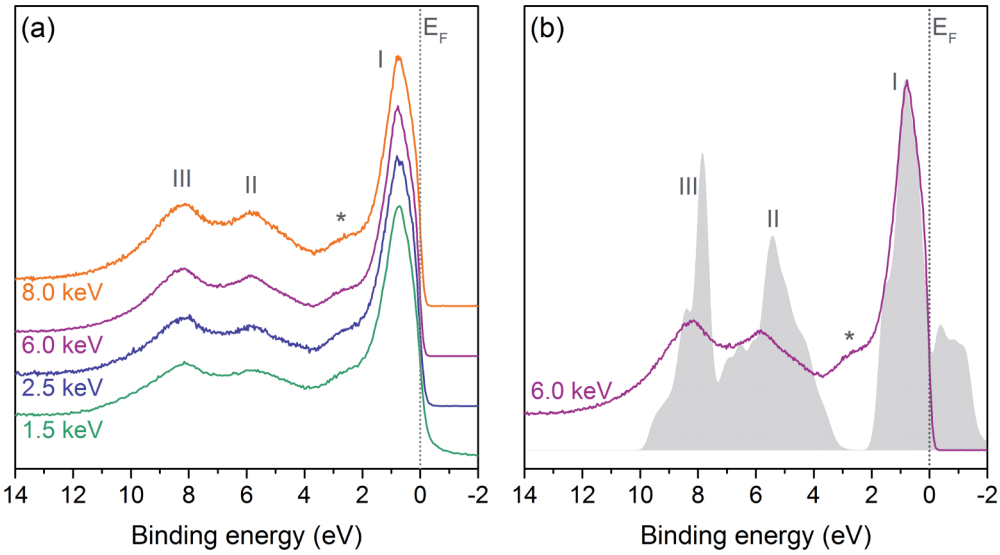

FIG. 4. Valence band spectra of OsO_2 (a) collected at varying photon energies and (b) collected at 6-keV excitation energy (line) and compared to the one-electron cross-section-weighted total density of states from DFT calculations (shaded).

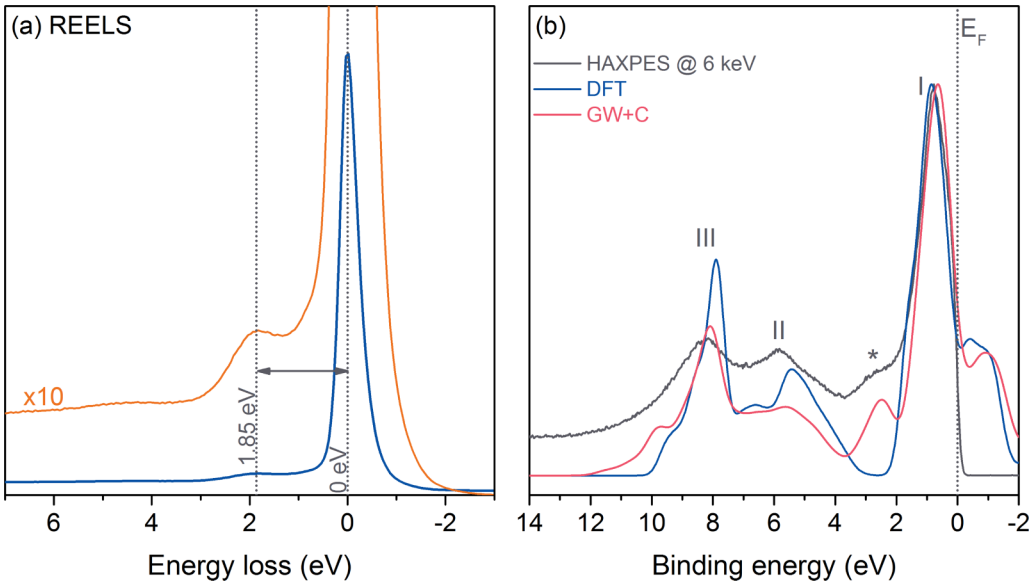

FIG. 6. Plasmon satellite feature within the valence band of OsO_2. (a) REELS spectrum. (b) Comparison of the experimental photoemission spectrum at 6 keV with the DFT and GW+C results.

the plasmon energy of OsO_2 using REELS, see Fig. 6(a). A clear plasmon feature at 1.85 eV above the main zero loss peak is observed. Using the experimentally measured plasmon energy, we have calculated the GW+C spectral function of OsO_2, see Fig. 6(b), and find it to be in good agreement with the experimental spectrum. In particular, the position of the feature marked by the asterisk is reproduced, indicating that it can be interpreted as a plasmon satellite, with an energy separation similar to that found for the core levels.

Although the plasmon model accounts for most aspects of the satellite structure, it must be noted that alternative approaches exist. These include dynamical mean-field theory, [52], and the Kotani local screening model [48]. The latter involves the Coulomb potential associated with a core hole pulling a state out of the conduction band to give a localized trapped state. A low-binding-energy screened final state arises from filling of the trapped state while for the unscreened final state at higher binding energy the trap remains empty. Despite discussion of the different screening models over many years [52–57], it remains a challenge to reconcile these approaches and to establish the contributions of the alternative mechanisms to valence and core hole screening.

In summary, this paper presents a comprehensive exploration of the electronic structure of osmium dioxide, which, due to the challenges in preparation, has received less attention than the other metallic rutile oxides. Both core-level and valence-band photoemission spectra have provided insights into the electronic structure of OsO_2, and in combination with theoretical calculations it is possible to identify all occupied state features in the spectroscopy results, including a low-energy plasmon satellite. These results form the basis for further investigations of this interesting metallic rutile oxide, and based on recent rapid developments in the field of iridates and ruthenates, this work on the parent oxide of the osmates, OsO_2, presents a case to further explore these fascinating materials.

We acknowledge the late Ying-Sheng Huang for providing the single crystals, which made this work possible. D.J.P. acknowledges support from the Royal Society (Grants No. UF100105 and No. UF150693). D.J.P. and A.R. acknowledge support from the EPSRC (Grant No. EP/M013839/1). The work at UCL was supported by EPSRC (EP/N01572X/1). D.J.P. and D.O.S. acknowledge membership of the Materials Design Network. A.M.G. acknowledges Diamond Light Source for the cosponsorship of a studentship on the EPSRC Centre for Doctoral Training in Molecular Modelling and Materials Science (Award No. EP/L015862/1). This work made use of the ARCHER UK National Supercomputing Service (http://www.archer.ac.uk) via the authors' membership of the UK's HEC Materials Chemistry Consortium, which was funded by EPSRC (Grant No. EP/L000202).

[1] W. Witczak-Krempa, G. Chen, Y. B. Kim, and L. Balents, Correlated quantum phenomena in the strong spin-orbit regime, Ann. Rev. Condens. Matter Phys. **5**, 57 (2014).

[2] J. G. Rau, E. K.-H. Lee, and H.-Y. Kee, Spin-orbit physics giving rise to novel phases in correlated systems: Iridates and related materials, Ann. Rev. Condens. Matter Phys. **7**, 195 (2016).

[3] S. Calder, J. G. Vale, N. A. Bogdanov, X. Liu, C. Donnerer, M. H. Upton, D. Casa, A. H. Said, M. D. Lumsden, Z. Zhao, J. Q. Yan, D. Mandrus, S. Nishimoto, J. van den Brink, J. P. Hill, D. F.

McMorrow, and A. D. Christianson, Spin-orbit-driven magnetic structure and excitation in the 5*d* pyrochlore $Cd_2Os_2O_7$, Nat. Commun. **7**, 11651 (2016).

[4] S. Calder, J. G. Vale, N. Bogdanov, C. Donnerer, D. Pincini, M. Moretti Sala, X. Liu, M. H. Upton, D. Casa, Y. G. Shi, Y. Tsujimoto, K. Yamaura, J. P. Hill, J. van den Brink, D. F. McMorrow, and A. D. Christianson, Strongly gapped spin-wave excitation in the insulating phase of $NaOsO_3$, Phys. Rev. B **95**, 020413 (2017).

[5] A. E. Taylor, S. Calder, R. Morrow, H. L. Feng, M. H. Upton, M. D. Lumsden, K. Yamaura, P. M. Woodward, and A. D. Christianson, Spin-Orbit Coupling Controlled $j = 3/2$ Electronic Ground State in $5d^3$ Oxides, Phys. Rev. Lett. **118**, 207202 (2017).

[6] S. Calder, D. J. Singh, V. O. Garlea, M. D. Lumsden, Y. G. Shi, K. Yamaura, and A. D. Christianson, Interplay of spin-orbit coupling and hybridization in Ca_3LiOsO_6 and Ca_3LiRuO_6, Phys. Rev. B **96**, 184426 (2017).

[7] L. F. Mattheiss, Electronic structure of RuO_2, OsO_2, and IrO_2, Phys. Rev. B **13**, 2433 (1976).

[8] M.-S. Miao and R. Seshadri, Rh_2O_3 versus IrO_2: Relativistic effects and the stability of Ir^{4+}, J. Phys.: Condens. Matter **24**, 215503 (2012).

[9] J. M. Kahk, C. G. Poll, F. E. Oropeza, J. M. Ablett, D. Céolin, J.-P. Rueff, S. Agrestini, Y. Utsumi, K. D. Tsuei, Y. F. Liao, F. Borgatti, G. Panaccione, A. Regoutz, R. G. Egdell, B. J. Morgan, D. O. Scanlon, and D. J. Payne, Understanding the Electronic Structure of IrO_2 using Hard-X-ray Photoelectron Spectroscopy and Density-Functional Theory, Phys. Rev. Lett. **112**, 117601 (2014).

[10] E. E. Rodriguez, F. Poineau, A. Llobet, A. P. Sattelberger, J. Bhattacharjee, U. V. Waghmare, T. Hartmann, and A. K. Cheetham, Structural studies of TcO_2 by neutron powder diffraction and first-principles calculations, J. Am. Chem. Soc. **129**, 10244 (2007).

[11] J. B. Goodenough, Metallic oxides, Prog. Solid State Chem. **5**, 145 (1971).

[12] Y. Sun, Y. Zhang, C.-X. Liu, C. Felser, and B. Yan, Dirac nodal lines and induced spin hall effect in metallic rutile oxides, Phys. Rev. B **95**, 235104 (2017).

[13] P. K. Das, J. Sławińska, I. Vobornik, J. Fujii, A. Regoutz, J. M. Kahk, D. O. Scanlon, B. J. Morgan, C. McGuinness, E. Plekhanov, D. Di Sante, Y.-S. Huang, R.-S. Chen, G. Rossi, S. Picozzi, W. R. Branford, G. Panaccione, and D. J. Payne, Role of spin-orbit coupling in the electronic structure of Iro_2, Phys. Rev. Mater. **2**, 065001 (2018).

[14] D. B. Rogers, R. D. Shannon, A. W. Sleight, and J. L. Gillson, Crystal chemistry of metal dioxides with rutile-related structures, Inorg. Chem. **8**, 841 (1969).

[15] P. C. Yen, R. S. Chen, C. C. Chen, Y. S. Huang, and K. K. Tiong, Growth and characterization of OsO_2 single crystals, J. Cryst. Growth **262**, 271 (2004).

[16] C.-E. Boman, Precision determination of the crystal structure of osmium dioxide, Acta Chem. Scand. **24**, 123 (1970).

[17] Y. Hayakawa, S. Kohiki, M. Arai, H. Yoshikawa, S. Fukushima, K. Wagatsuma, M. Oku, and F. Shoji, Electronic structure and electrical properties of amorphous OsO_2, Phys. Rev. B **59**, 11125 (1999).

[18] G. Kresse and J. Hafner, *Ab initio* molecular-dynamics simulation of the liquid-metal? amorphous-semiconductor transition in germanium, Phys. Rev. B **49**, 14251 (1994).

[19] G. Kresse and J. Furthmüller, Efficiency of ab-initio total energy calculations for metals and semiconductors using a plane-wave basis set, Comput. Mater. Sci. **6**, 15 (1996).

[20] G. Kresse and J. Hafner, *Ab initio* molecular dynamics for liquid metals, Phys. Rev. B **47**, 558 (1993).

[21] G. Kresse and J. Furthmüller, Efficient iterative schemes for ab initio total-energy calculations using a plane-wave basis set, Phys. Rev. B **54**, 11169 (1996).

[22] G. Kresse and D. Joubert, From ultrasoft pseudopotentials to the projector augmented-wave method, Phys. Rev. B **59**, 1758 (1999).

[23] J. P. Perdew, A. Ruzsinszky, G. I. Csonka, O. A. Vydrov, G. E. Scuseria, L. A. Constantin, X. Zhou, and K. Burke, Restoring the Density-Gradient Expansion for Exchange in Solids and Surfaces, Phys. Rev. Lett. **100**, 136406 (2008).

[24] J. P. Perdew, K. Burke, and M. Ernzerhof, Generalized Gradient Approximation Made Simple, Phys. Rev. Lett. **77**, 3865 (1996).

[25] A. M. Ganose and D. O. Scanlon, Band gap and work function tailoring of SnO_2 for improved transparent conducting ability in photovoltaics, J. Mater. Chem. C **4**, 1467 (2016).

[26] N. F. Quackenbush, H. Paik, M. J. Wahila, S. Sallis, M. E. Holtz, X. Huang, A. Ganose, B. J. Morgan, D. O. Scanlon, Y. Gu, F. Xue, L.-Q. Chen, G. E. Sterbinsky, C. Schlueter, T.-L. Lee, J. C. Woicik, J.-H. Guo, J. D. Brock, D. A. Muller, D. A. Arena, D. G. Schlom, and L. F. J. Piper, Stability of the M2 phase of vanadium dioxide induced by coherent epitaxial strain, Phys. Rev. B **94**, 085105 (2016).

[27] D. Hobbs, G. Kresse, and J. Hafner, Fully unconstrained noncollinear magnetism within the projector augmented-wave method, Phys. Rev. B **62**, 11556 (2000).

[28] F. Aryasetiawan, L. Hedin, and K. Karlsson, Multiple Plasmon Satellites in Na and Al Spectral Functions from *Ab Initio* Cumulant Expansion, Phys. Rev. Lett. **77**, 2268 (1996).

[29] M. Guzzo, G. Lani, F. Sottile, P. Romaniello, M. Gatti, J. J. Kas, J. J. Rehr, M. G. Silly, F. Sirotti, and L. Reining, Valence Electron Photoemission Spectrum of Semiconductors: *Ab Initio* Description of Multiple Satellites, Phys. Rev. Lett. **107**, 166401 (2011).

[30] M. Guzzo, J. J. Kas, F. Sottile, M. G. Silly, F. Sirotti, J. J. Rehr, and L. Reining, Plasmon satellites in valence-band photoemission spectroscopy, Eur. Phys. J. B **85**, 324 (2012).

[31] J. Lischner, G. K. Pálsson, D. Vigil-Fowler, S. Nemsak, J. Avila, M. C. Asensio, C. S. Fadley, and S. G. Louie, Satellite band structure in silicon caused by electron-plasmon coupling, Phys. Rev. B **91**, 205113 (2015).

[32] J. S. Zhou, M. Gatti, J. J. Kas, J. J. Rehr, and L. Reining, Cumulant green's function calculations of plasmon satellites in bulk sodium: Influence of screening and the crystal environment, Phys. Rev. B **97**, 035137 (2018).

[33] M. Gatti, G. Panaccione, and L. Reining, Effects of Low-Energy Excitations on Spectral Properties at Higher Binding Energy: The Metal-Insulator Transition of VO_2, Phys. Rev. Lett. **114**, 116402 (2015).

[34] K. Nakamura, Y. Nohara, Y. Yosimoto, and Y. Nomura, *Ab initio GW* plus cumulant calculation for isolated band systems:

Application to organic conductor $(TMTSF)_2PF_6$ and transition-metal oxide $SrVO_3$, Phys. Rev. B **93**, 085124 (2016).

[35] F. Caruso, H. Lambert, and F. Giustino, Band Structures of Plasmonic Polarons, Phys. Rev. Lett. **114**, 146404 (2015).

[36] J. Lischner, D. Vigil-Fowler, and Steven G Louie, Physical Origin of Satellites in Photoemission of Doped Graphene: An *Ab Initio GW* Plus Cumulant Study, Phys. Rev. Lett. **110**, 146801 (2013).

[37] F. Borgatti, J. A. Berger, D. Céolin, J. S. Zhou, J. J. Kas, M. Guzzo, C. F. McConville, F. Offi, G. Panaccione, A. Regoutz, D. J. Payne, J.-P. Rueff, O. Bierwagen, M. E. White, J. S. Speck, M. Gatti, and R. G. Egdell, Revisiting the origin of satellites in core-level photoemission of transparent conducting oxides: The case of *n*-doped SnO_2, Phys. Rev. B **97**, 155102 (2018).

[38] J. Deslippe, G. Samsonidze, D. A. Strubbe, M. Jain, M. L. Cohen, and S. G. Louie, Berkeley*GW*: A massively parallel computer package for the calculation of the quasiparticle and optical properties of materials and nanostructures, Comput. Phys. Commun. **183**, 1269 (2012).

[39] The DFT calculations for the GW+C calculations employed norm-conserving Troullier-Martins pseudopotentials, a plane-wave cutoff of 100 Ry, and a shifted $6 \times 6 \times 8$ Monkhort-Pack *k*-point grid and were carried out using the Quantum Espresso software package.

[40] Y. C. Venudhar, L. Iyengar, and K. V. Krishna Rao, Anomalous thermal expansion of osmium dioxide, Cryst. Res. Technol. **20**, 1393 (1985).

[41] A. J. Jackson, A. M. Ganose, A. Regoutz, R. G. Egdell, and D. O. Scanlon, Galore: Broadening and weighting for simulation of photoelectron spectroscopy, J. Open Source Softw. **3**, 773 (2018).

[42] See Supplemental Material at http://link.aps.org/supplemental/10.1103/PhysRevMaterials.3.025001 for one-electron cross sections of Os and O.

[43] D. D. Sarma and C. N. R. Rao, Xpes studies of oxides of second- and third-row transition metals including rare earths, J. Electron Spectrosc. Relat. Phenom. **20**, 25 (1980).

[44] D. J. Payne, R. G. Egdell, W. Hao, J. S. Foord, A. Walsh, and G. W. Watson, Why is lead dioxide metallic? Chem. Phys. Lett. **411**, 181 (2005).

[45] C. Körber, V. Krishnakumar, A. Klein, G. Panaccione, P. Torelli, A. Walsh, J. L. F. Da Silva, S.-H. Wei, R. G. Egdell, and D. J. Payne, Electronic structure of In_2O_3 and sn-doped In_2O_3 by hard x-ray photoemission spectroscopy, Phys. Rev. B **81**, 165207 (2010).

[46] J. N. Chazalviel, M. Campagna, G. K. Wertheim, and H. R. Shanks, Final-state effects in the x-ray photoelectron spectra of cubic sodium-tungsten bronzes, Phys. Rev. B **16**, 697 (1977).

[47] D. O. Scanlon, G. W. Watson, D. J. Payne, G. R. Atkinson, R. G. Egdell, and D. S. L. Law, Theoretical and experimental study of the electronic structures of MoO_3 and MoO_2, J. Phys. Chem. C **114**, 4636 (2010).

[48] A. Kotani, Theoretical studies on core-level spectra of solids, J. Electron Spectrosc. Relat. Phenom. **78**, 7 (1996).

[49] A. Bourlange, D. J. Payne, R. G. Palgrave, H. Zhang, J. S. Foord, R. G. Egdell, R. M. J. Jacobs, T. D. Veal, P. D. C. King, and C. F. McConville, The influence of sn doping on the growth of In_2O_3 on Y-stabilized $ZrO_2(100)$ by oxygen plasma assisted molecular beam epitaxy, J. Appl. Phys. **106**, 013703 (2009).

[50] J. J. Mudd, T.-L. Lee, V. Muñoz-Sanjosé, J. Zúñiga-Pérez, D. Hesp, J. M. Kahk, D. J. Payne, R. G. Egdell, and C. F. McConville, Hard x-ray photoelectron spectroscopy as a probe of the intrinsic electronic properties of CdO, Phys. Rev. B **89**, 035203 (2014).

[51] K. Fujiwara, Y. Fukuma, J. Matsuno, H. Idzuchi, Y. Niimi, Y. Otani, and H. Takagi, Diridium oxide as a material for spin-current detection, Nat. Commun. **4**, 1 (2013).

[52] H. D. Kim, H. J. Noh, K. H. Kim, and S. J. Oh, Core-Level X-Ray Photoemission Satellites in Ruthenates: A New Mechanism Revealing The Mott Transition, Phys. Rev. Lett. **93**, 126404 (2004).

[53] R. G. Egdell, H. Innes, and M. D. Hill, Electronic and structural study of $Na_{2/3}WO_3(110)$ by XPS, UPS, EELS and LEED, Surf. Sci. **149**, 33 (1985).

[54] F. Werfel and E. Minni, Photoemission study of the electronic structure of Mo and Mo oxides, J. Phys. C: Solid State Phys. **16**, 6091 (1983).

[55] G. K. Wertheim, L. F. Schneemeyer, and D. N. E. Buchanan, Energy band and final-state effects in $K_{0.30}$ MoO_3, Phys. Rev. B **32**, 3568 (1985).

[56] H. Wadati, J. Mravlje, K. Yoshimatsu, H. Kumigashira, M. Oshima, T. Sugiyama, E. Ikenaga, A. Fujimori, A. Georges, A. Radetinac, K. S. Takahashi, M. Kawasaki, and Y. Tokura, Photoemission and DMFT study of electronic correlations in $SrMoO_3$: Effects of Hund's rule coupling and possible plasmonic sideband, Phys. Rev. B **90**, 205131 (2014).

[57] G. K. Wertheim, L. F. Mattheiss, M. Campagna, and T. P. Pearsall, Transition Probabilities and Overlap-Covalency Effects in the X-ray Photoemission Spectra of Transition-Metal Compounds: ReO_3, Phys. Rev. Lett. **32**, 997 (1974).